

Terahertz Sources Based on Intra-Cavity Difference-Frequency Generation in Quantum Cascade Lasers

Mikhail A. Belkin¹, Federico Capasso¹,
Feng Xie², Alexey Belyanin²,
Deborah L. Sivco³
Milan Fischer⁴, Jérôme Faist⁴,
Douglas C. Oakley⁵, Christopher J. Vineis⁵, George W.
Turner⁵

1. *Harvard School of Engineering and Applied Sciences*
2. *Physics Department, Texas A&M University*
3. *Bell Laboratories*
4. *ETH, Zurich*
5. *MIT Lincoln Laboratory*

Motivation



Compact THz source

- Injection pumped
- CW at TE cooler temperature
- Widely tunable
- $\sim 10\text{-}1000\mu\text{W}$ of CW THz power

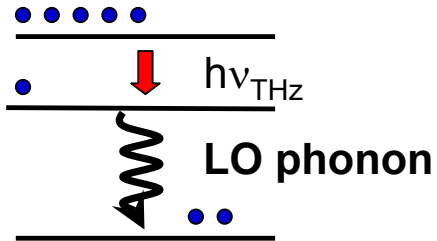
Applications

- Spectroscopy
- Local oscillator for THz heterodyning
- Remote sensing, screening, inspection

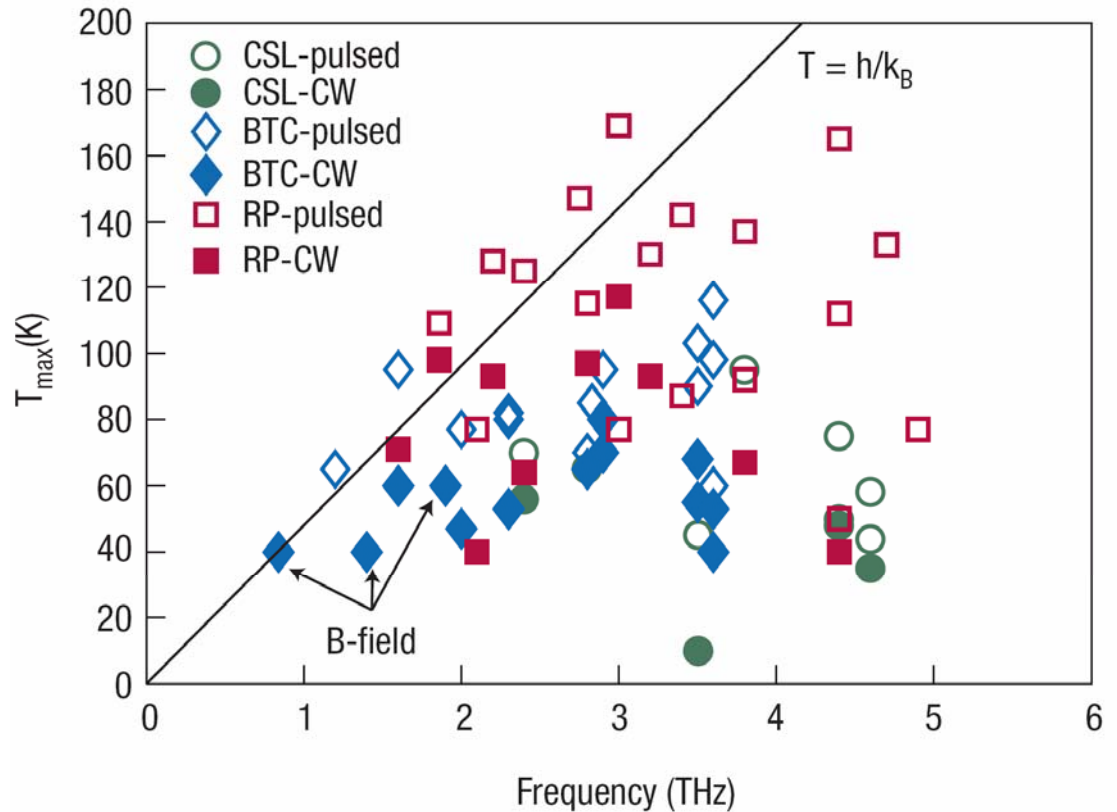
THz QCL



T_{max} vs frequency



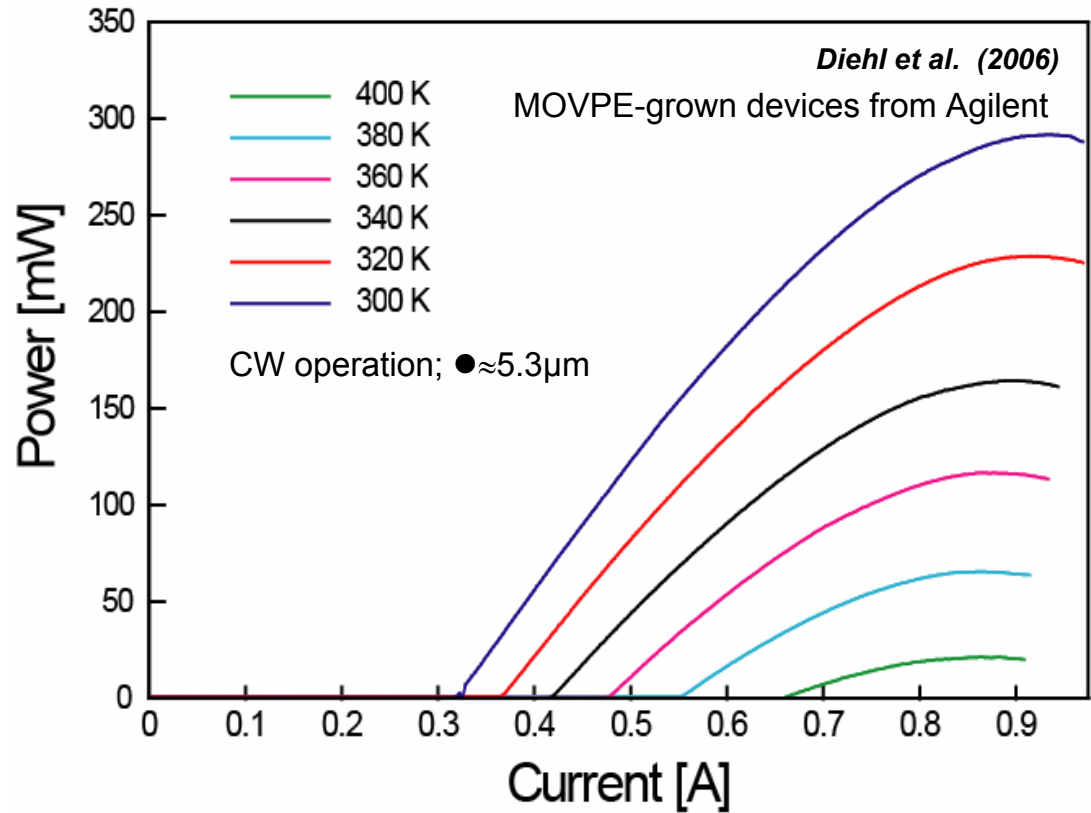
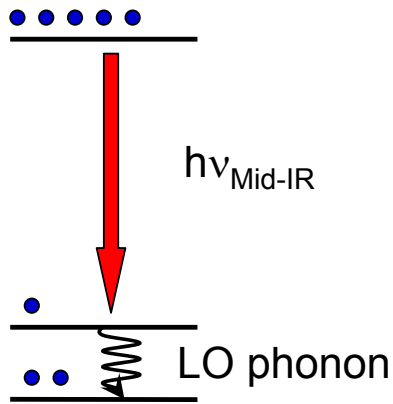
Nonradiative decay rates grow quickly with temperature in THz QCLs



Mid-IR QCL



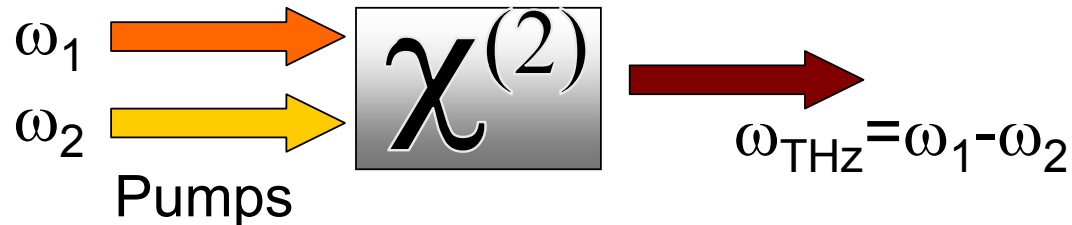
Excellent performance in mid-infrared



THz Difference Frequency Generation

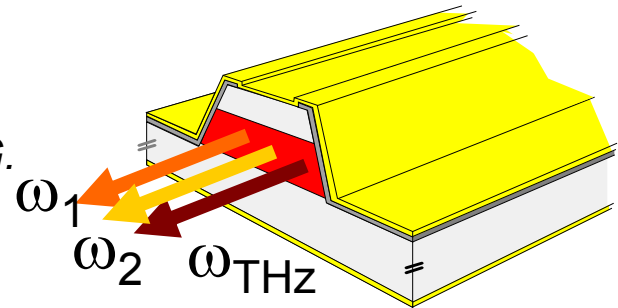


Difference-frequency generation (DFG) occurs in a medium with second-order nonlinear susceptibility $\chi^{(2)}$



THz QCL source using intra-cavity DFG

- Dual-frequency mid-infrared QCLs with monolithically integrated $\chi^{(2)}$.
- THz radiation is generated via intra-cavity DFG.
- Widely tunable THz source at RT (using DFB gratings for both pump lasers).



Challenges for intra-cavity THz DFG



$$I(\omega_{THz}) \propto |\chi^{(2)}|^2 I(\omega_1) I(\omega_2) \times l_{eff}^2$$

Traditional schemes for THz DFG:

Use high-intensity pumps from pulsed solid-state lasers (up to 1GW/cm²)

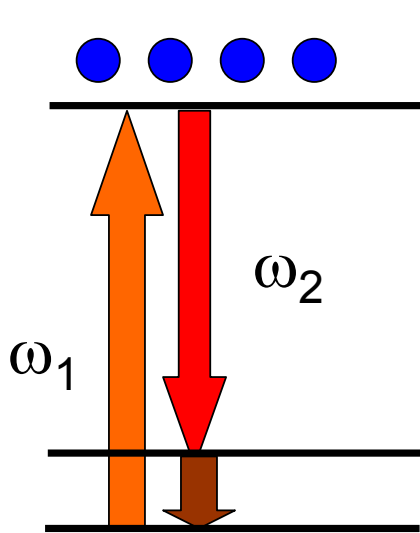
and/or

Utilize long l_{eff} (tens of mm) in transparent nonlinear crystals

Intra-cavity THz DFG in dual-wavelength mid-IR QCL:

- Relatively low pump intensities (up to 1-10MW/cm²)
- l_{eff} is limited by free-carrier absorption to ≈ 0.2 mm
- Quantum well structures may have **giant** $\chi^{(2)}$ (up to 10⁶ pm/V)

$\chi^{(2)}$ with population inversion

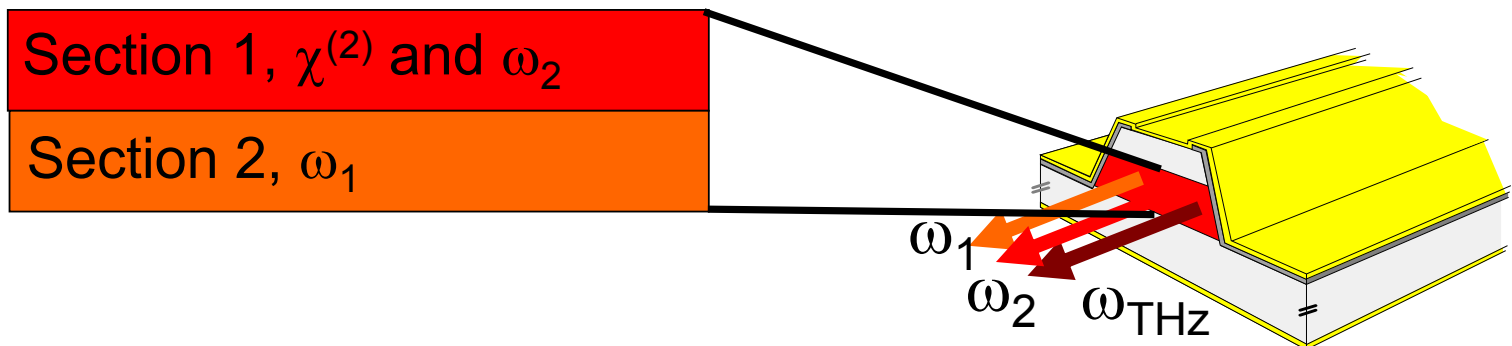


$$\chi^{(2)}(\omega=\omega_1-\omega_2) \sim \sum_{n,n'} \frac{z_{1n} z_{nn'} z_{n'1}}{(\omega-\omega_{nn'}+i\Gamma_{nn'})} \left(\frac{1}{(\omega_1+\omega_{n'1}+i\Gamma_{n'1})} + \frac{1}{(-\omega_2-\omega_{n1}+i\Gamma_{n1})} \right)$$

Quantum cascade laser structure with giant $\chi^{(2)}$.

- Giant $\chi^{(2)}$ with population inversion
- Laser action instead of absorption

Active region design

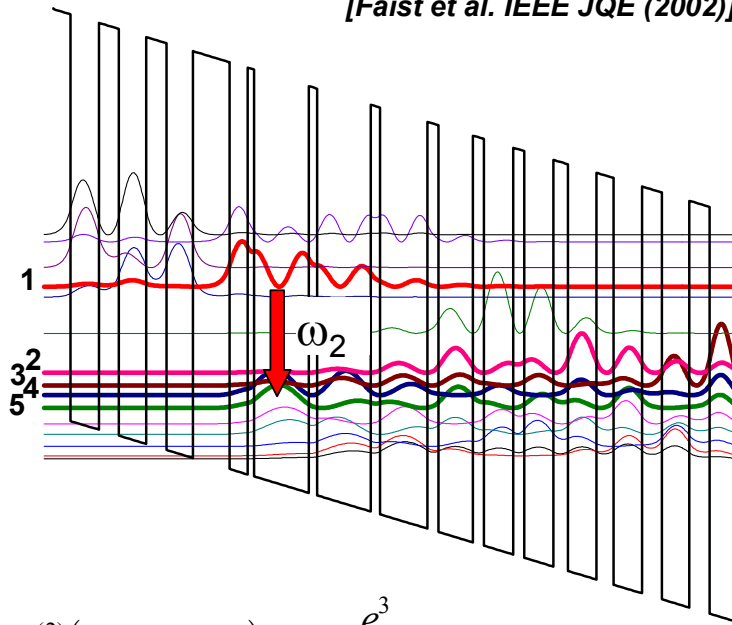


$\chi^{(2)}$ -section design



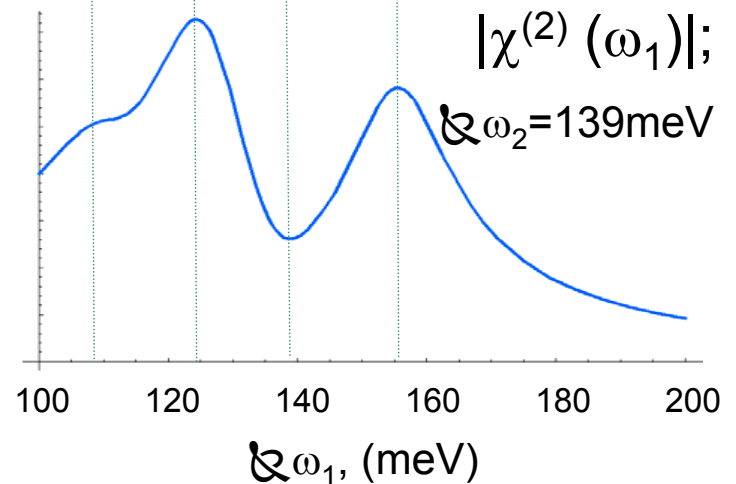
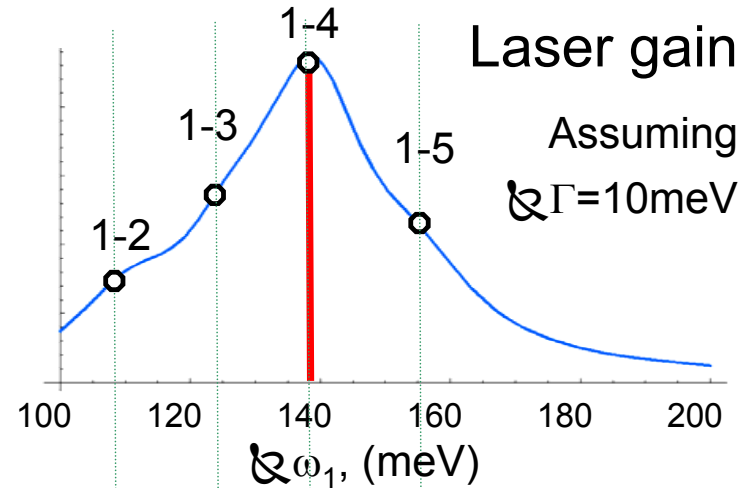
Bound-to-continuum active region for $\lambda \approx 9\mu\text{m}$

[Faist et al. IEEE JQE (2002)]



$$\chi^{(2)}(\omega = \omega_1 - \omega_2) \approx N_e \frac{e^3}{\hbar^2 \epsilon_0} \times$$

$$\sum_{n,n'} \frac{z_{1n} z_{nm'} z_{n'1}}{(\omega - \omega_{nm'} + i\Gamma_{nm'})} \left(\frac{1}{(\omega_1 + \omega_{n'1} + i\Gamma_{n'1})} + \frac{1}{(-\omega_2 - \omega_{n1} + i\Gamma_{n1})} \right)$$

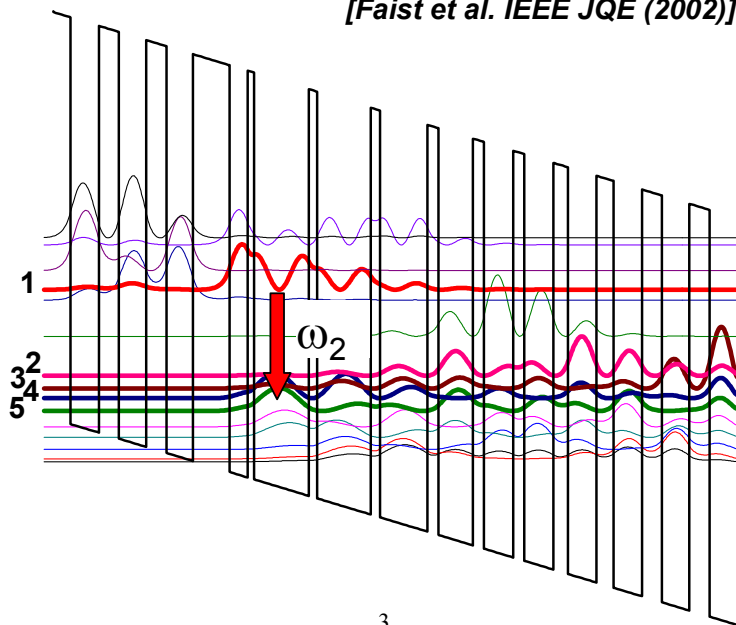


$\chi^{(2)}$ -section design



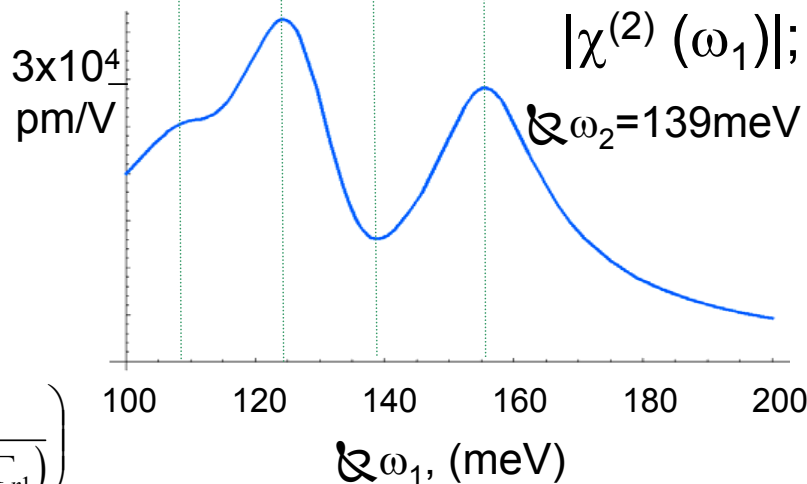
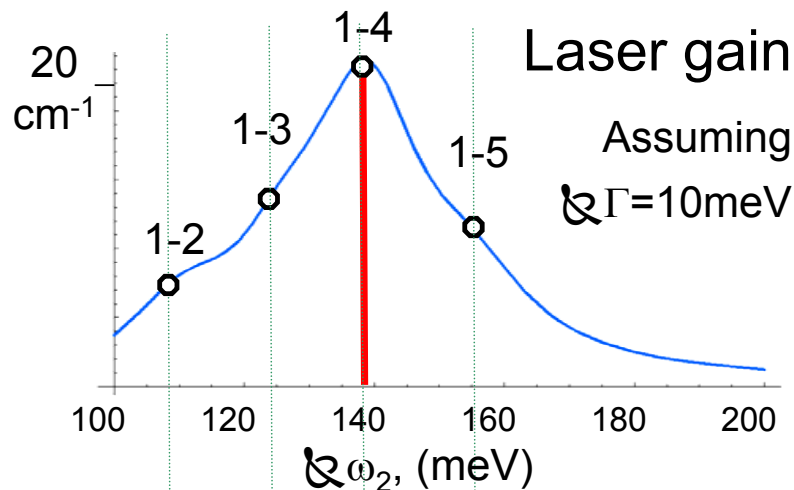
Bound-to-continuum active region for $\lambda \approx 9\mu\text{m}$

[Faist et al. IEEE JQE (2002)]

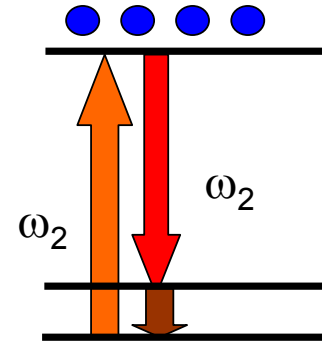
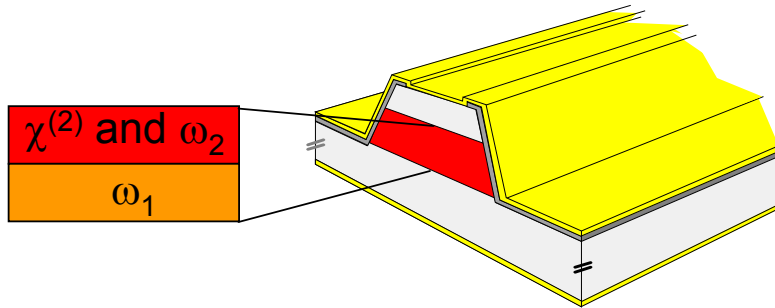


$$\chi^{(2)}(\omega = \omega_1 - \omega_2) \approx N_e \frac{e^3}{\hbar^2 \epsilon_0} \times$$

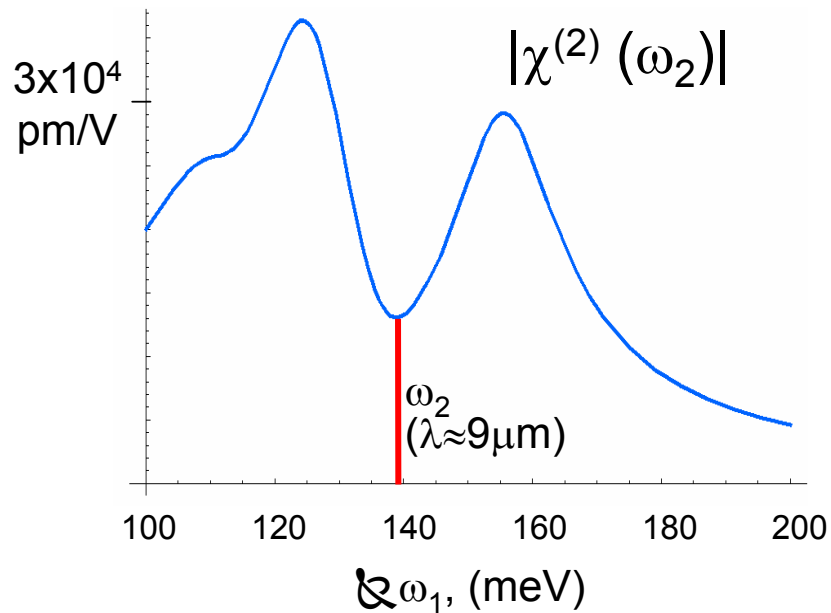
$$\sum_{n,n'} \frac{z_{1n} z_{nm'} z_{n'1}}{(\omega - \omega_{nm'} + i\Gamma_{nm'})} \left(\frac{1}{(\omega_1 + \omega_{n'1} + i\Gamma_{n'1})} + \frac{1}{(-\omega_2 - \omega_{n1} + i\Gamma_{n1})} \right)$$



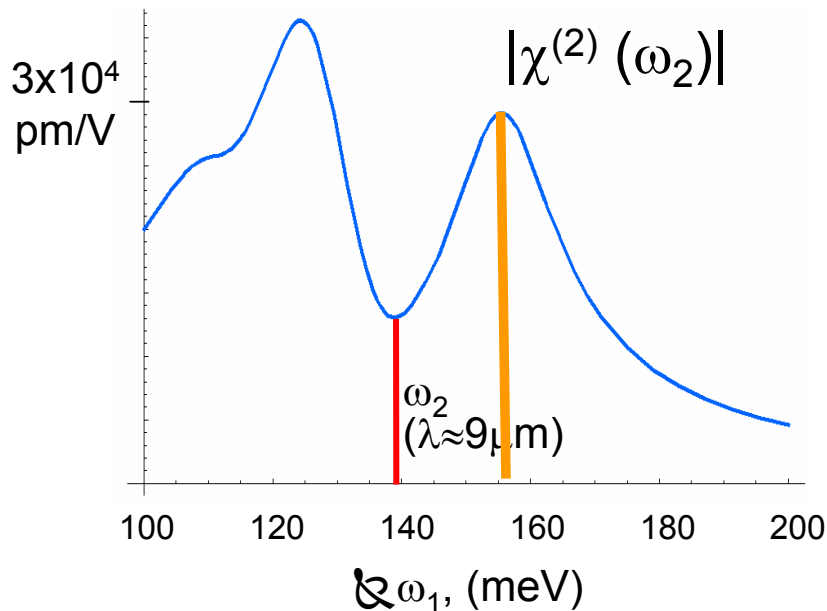
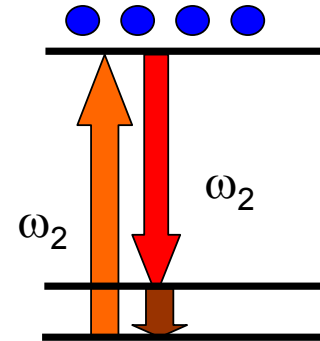
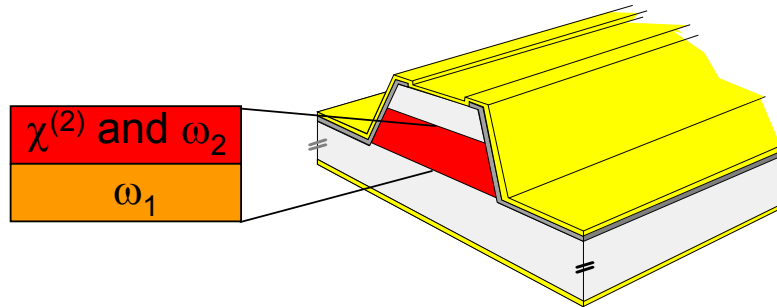
Active region design



Section with ω_1 :



Active region design

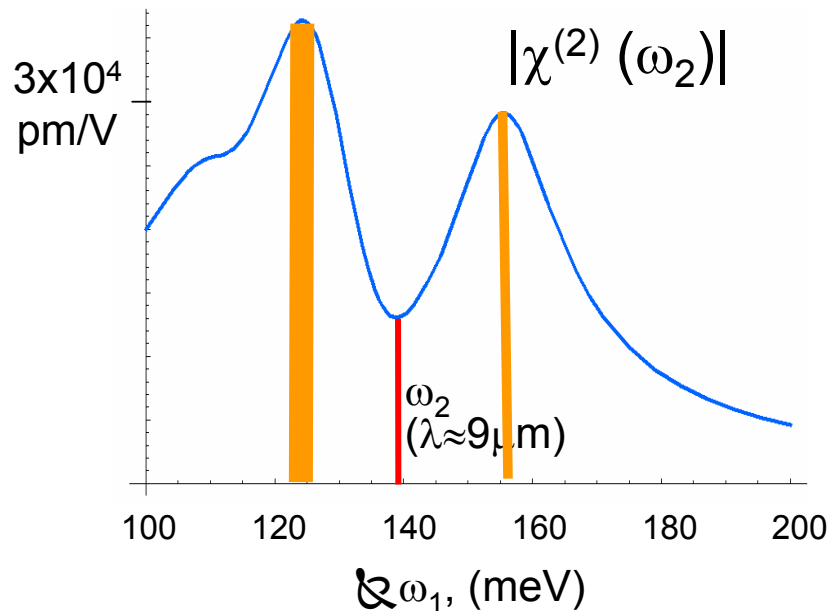
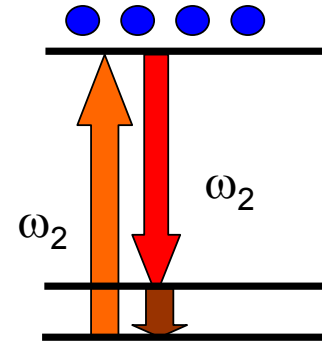
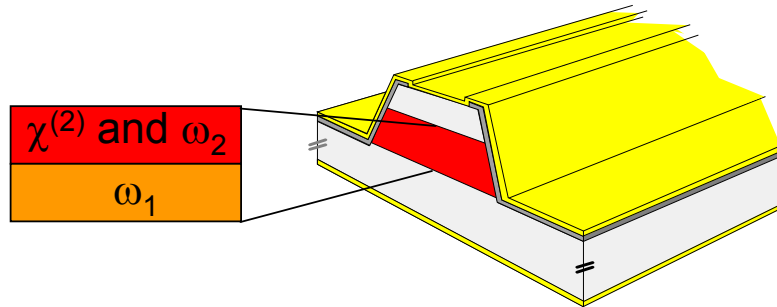


Section with ω_1 :

1. Two-phonon design at 155meV ($\lambda \approx 8\mu\text{m}$)

[Nature Photonics 1, 288 (2007)]

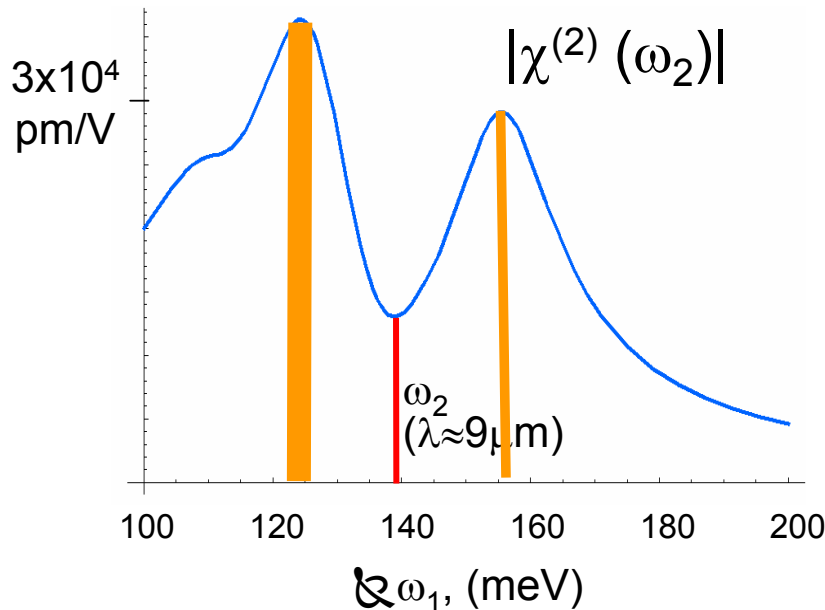
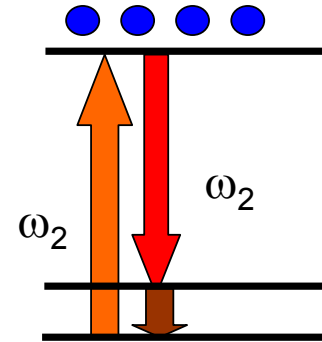
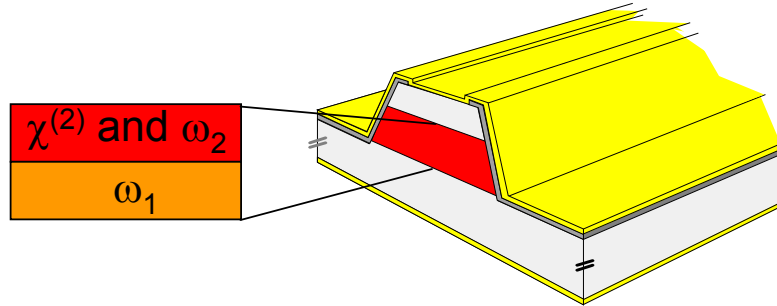
Active region design



Section with ω_1 :

1. Two-phonon design at 155meV ($\lambda \approx 8 \mu\text{m}$)
[Nature Photonics 1, 288 (2007)]
2. Two-phonon design at 125meV ($\lambda \approx 10 \mu\text{m}$)

Active region design



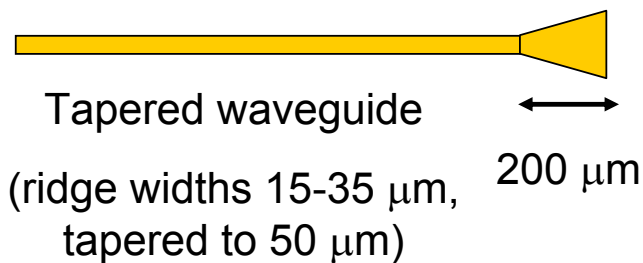
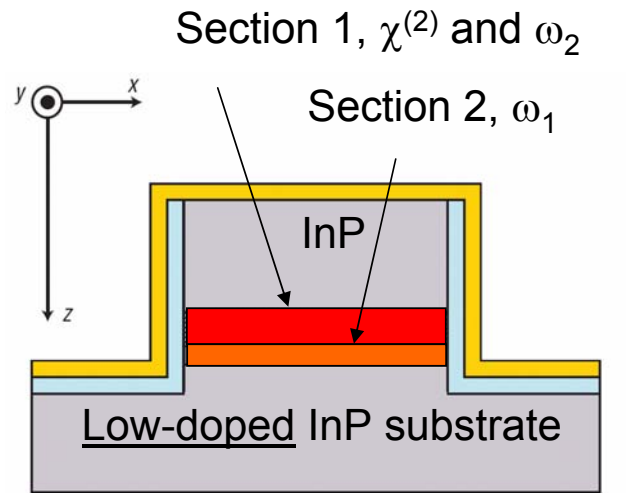
Section with ω_1 :

1. Two-phonon design at 155meV
($\lambda \approx 8\mu\text{m}$)

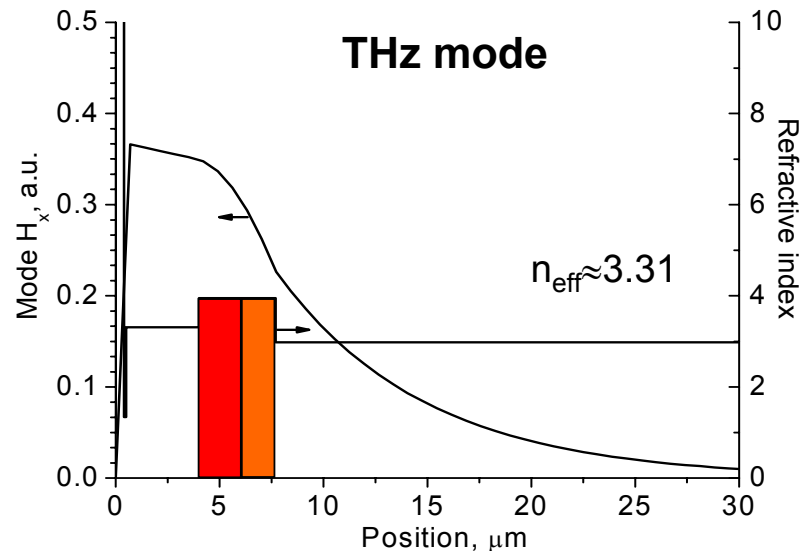
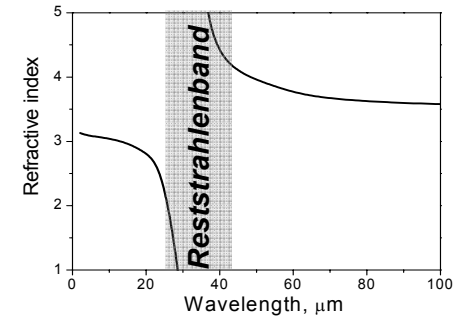
[Nature Photonics 1, 288 (2007)]

2. Two-phonon design at 125meV
($\lambda \approx 10\mu\text{m}$)

Waveguide design



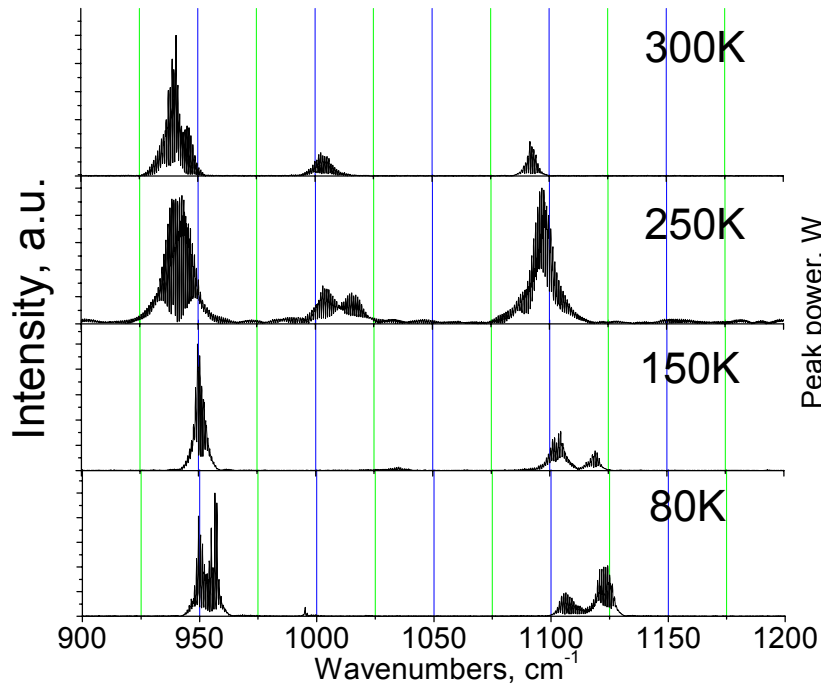
- Dielectric waveguide for mid-IR modes
- Surface plasmon waveguide for THz mode
- Good THz out-coupling
- Close to phase matching due to Reststrahlenband
- $l_{\text{eff}} \approx 70 \mu\text{m}$ for DFG



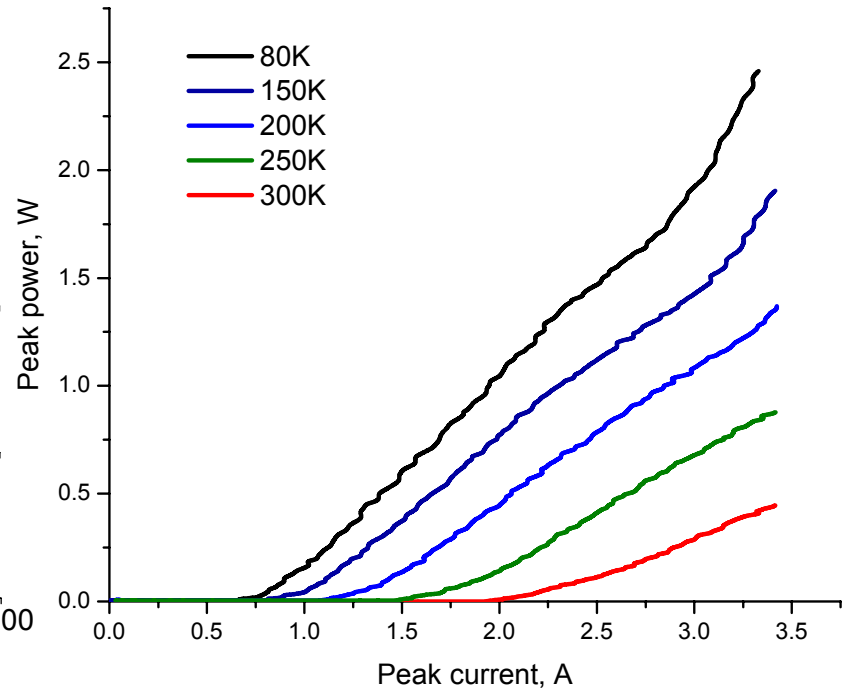
Device performance: mid-IR



Spectra



Power (combined)

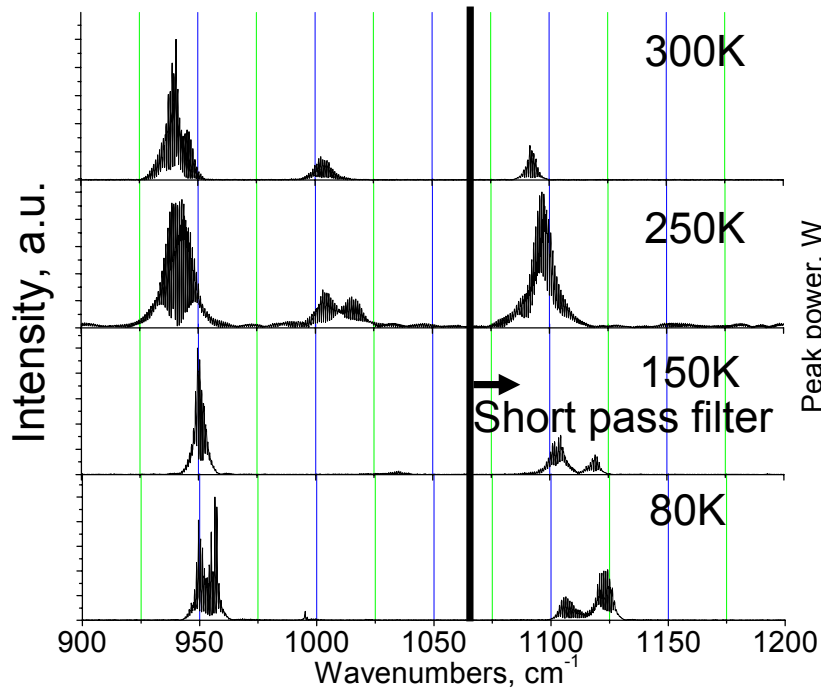


25- μm -wide, tapered to 50- μm -wide, 2-mm-long, back facet HR coating.
Testing in pulsed mode (60ns pulses at 250kHz).

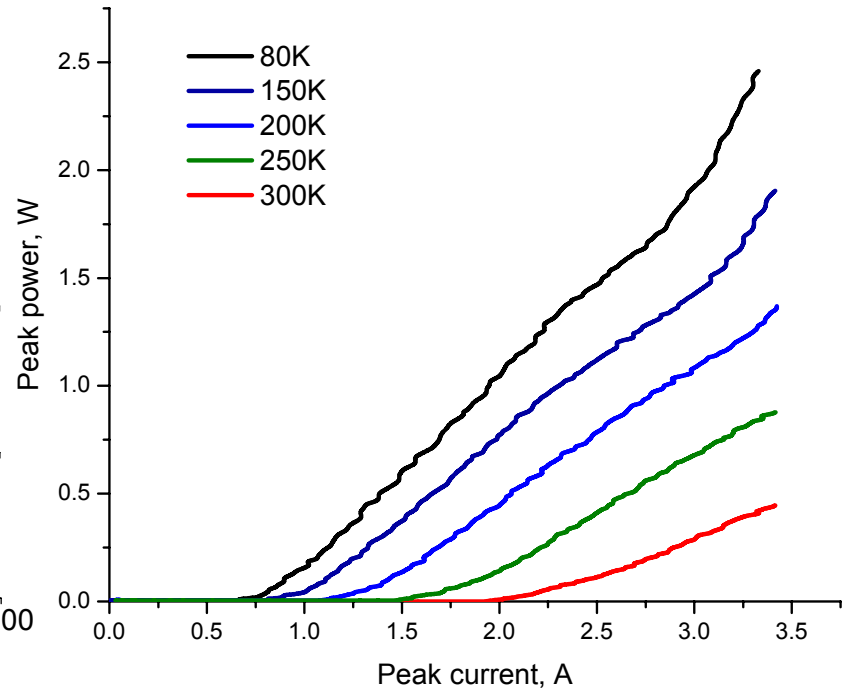
Device performance: mid-IR



Spectra



Power (combined)

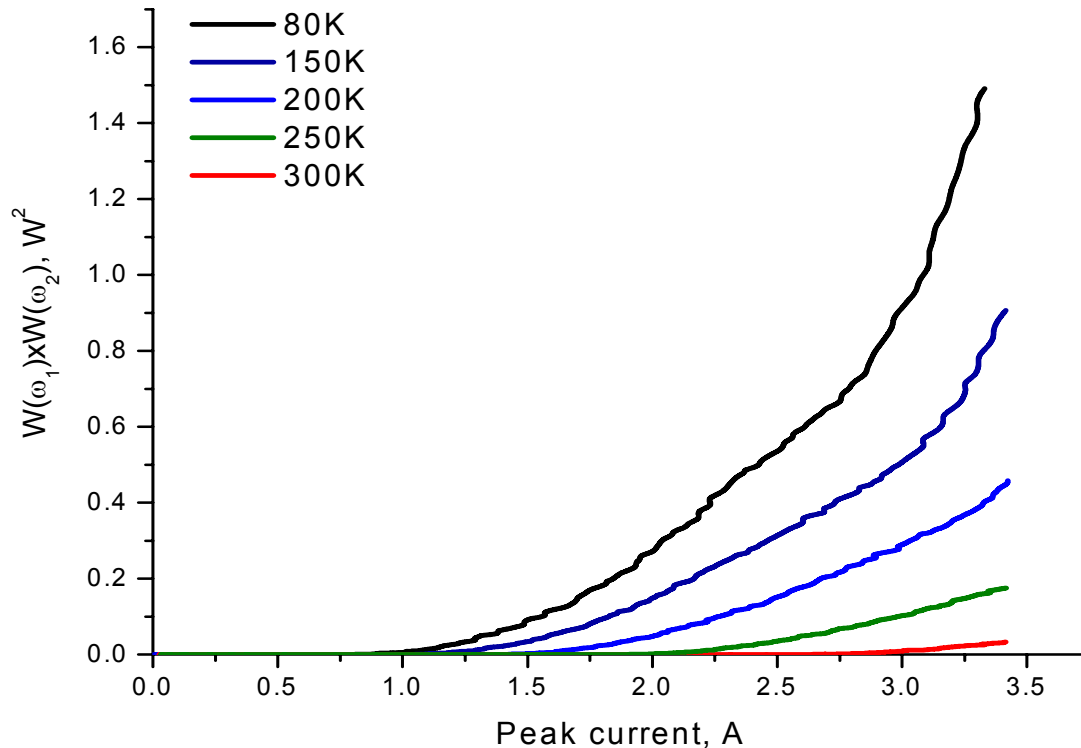


25- μm -wide, tapered to 50- μm -wide, 2-mm-long, back facet HR coating.
Testing in pulsed mode (60ns pulses at 250kHz).

Product of the pump powers



$$W(\omega_{THz}) \propto |\chi^{(2)}|^2 W(\omega_1)W(\omega_2) \times l_{eff}^2$$

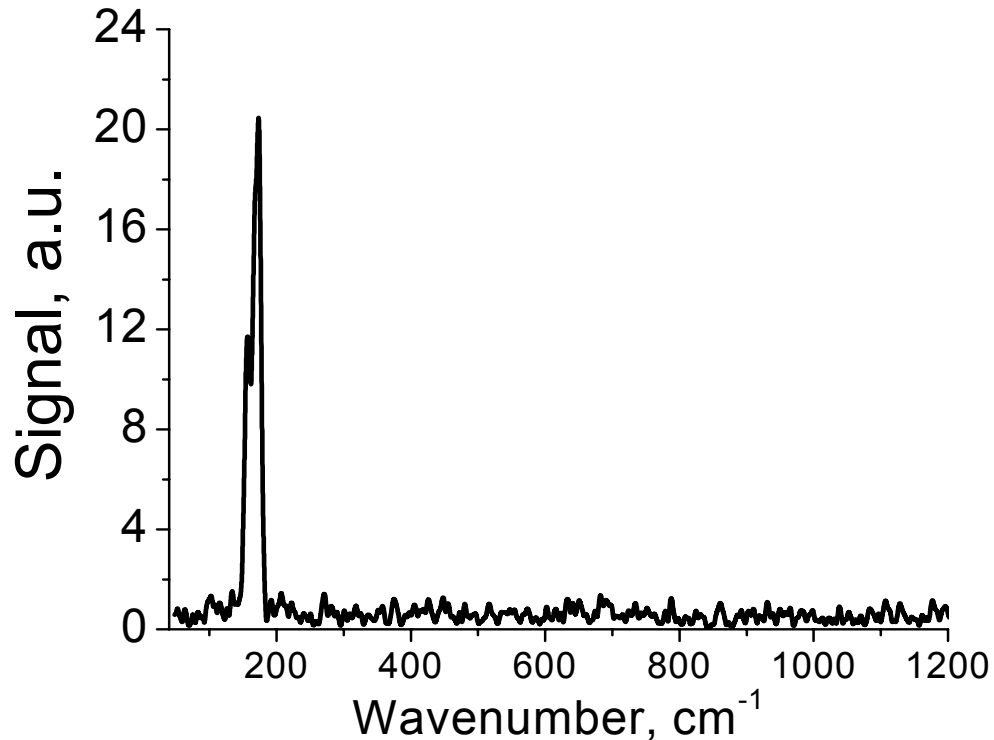


25- μ m-wide, tapered to 50- μ m-wide, 2-mm-long, back facet HR coating.
Testing in pulsed mode (60ns pulses at 250kHz).

Terahertz emission 80K

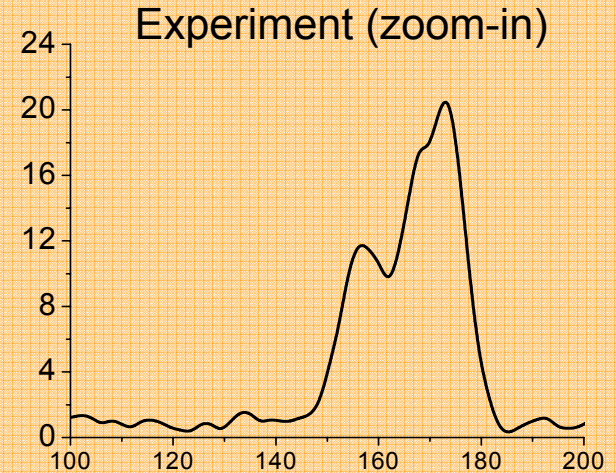
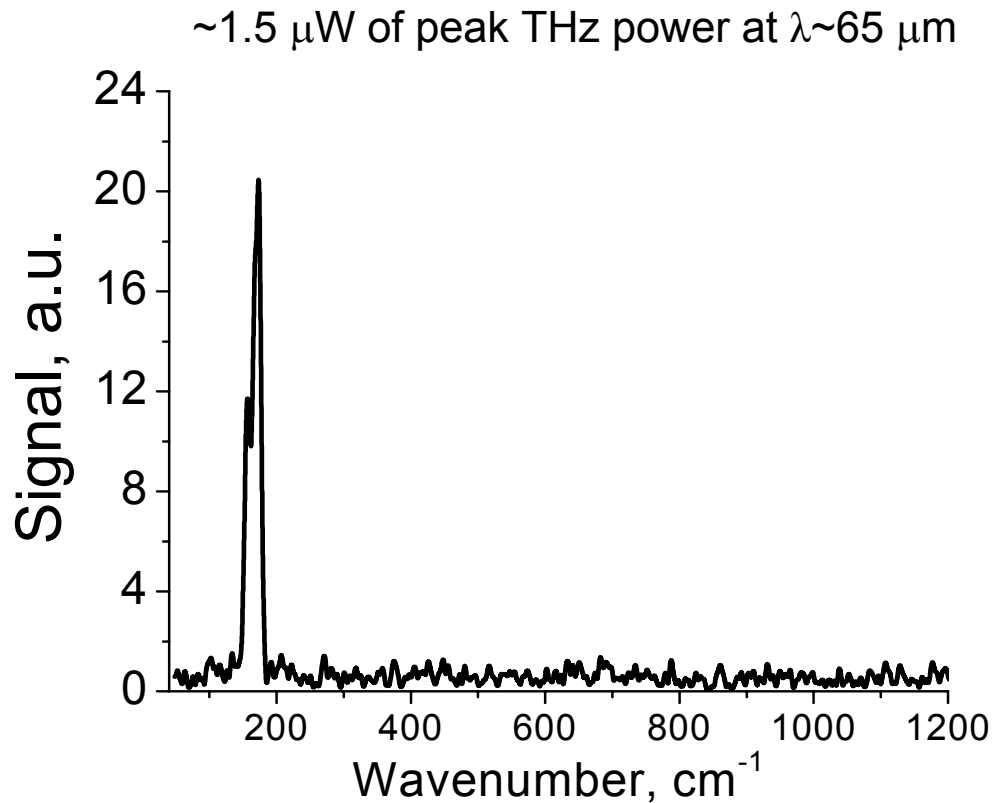


~1.5 μW of peak THz power at $\lambda \sim 65 \mu\text{m}$

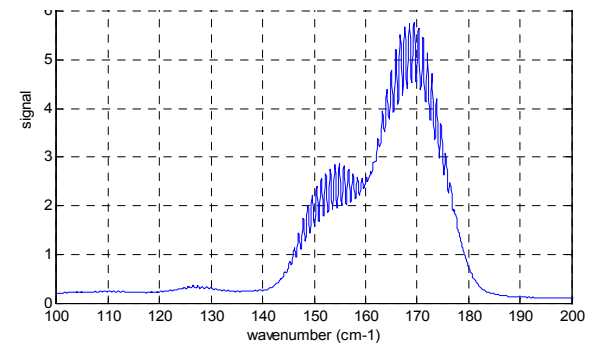


25- μm -wide, tapered to 50- μm -wide, 2-mm-long, back facet HR coating.
Testing in pulsed mode (60ns pulses at 250kHz).

Terahertz emission 80K

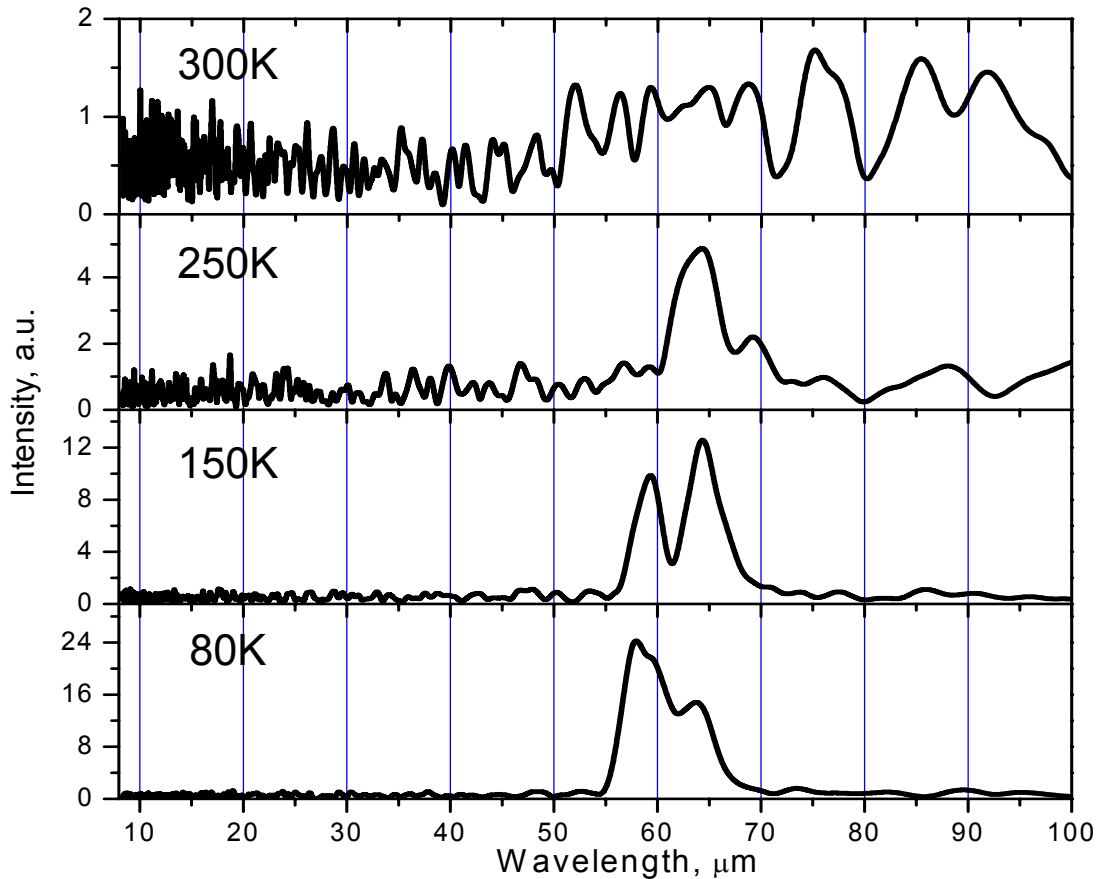


Simulations from mid-IR data



25- μm -wide, tapered to 50- μm -wide, 2-mm-long, back facet HR coating.
Testing in pulsed mode (60ns pulses at 250kHz).

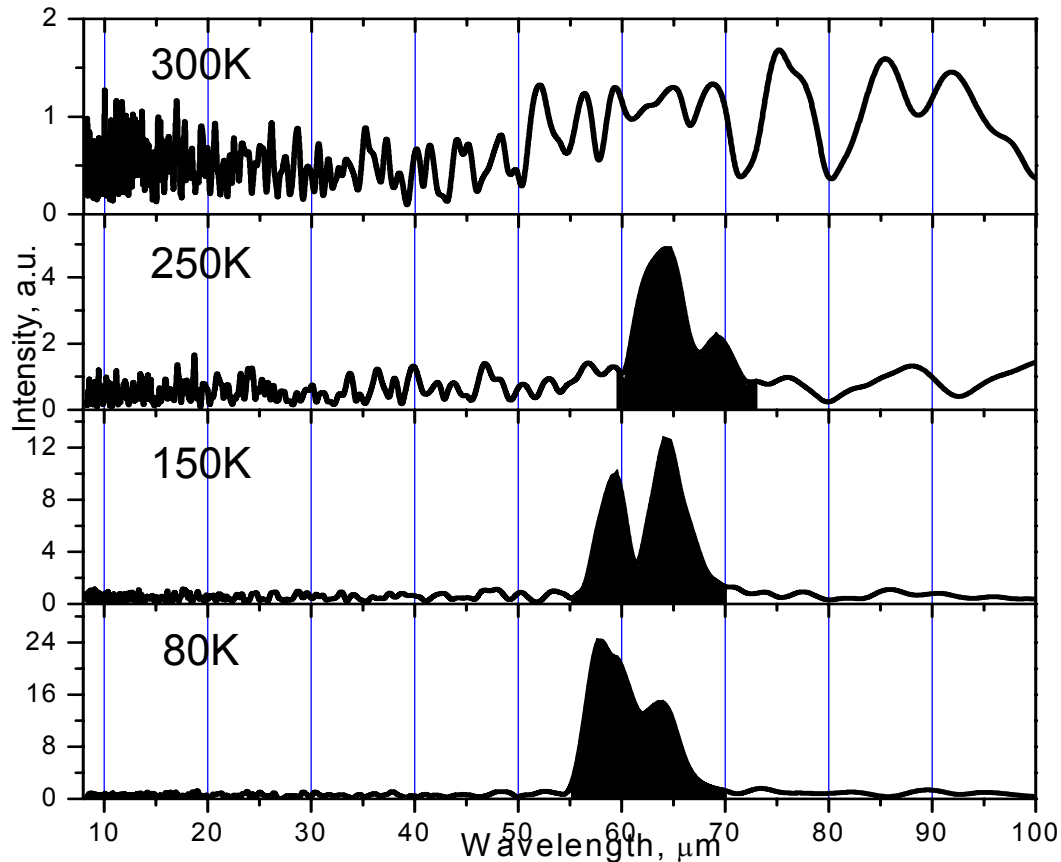
Terahertz emission different T



- Peak positions agree with mid-IR data
- Red-shift with temperature can also be observed in mid-IR data
- THz DFG signal observed up to 250K

25- μm -wide, tapered to 50- μm -wide, 2-mm-long, back facet HR coating.
Testing in pulsed mode (60ns pulses at 250kHz).

Terahertz emission



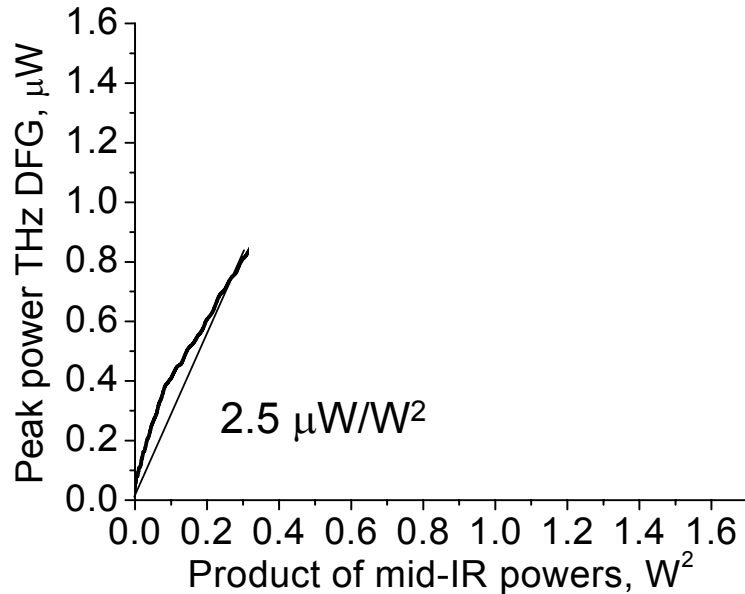
- Peak positions agree with mid-IR data
- Red-shift with temperature can also be observed in mid-IR data
- THz DFG signal observed up to 250K

25- μm -wide, tapered to 50- μm -wide, 2-mm-long, back facet HR coating.
Testing in pulsed mode (60ns pulses at 250kHz).

THz power/conversion efficiency



THz DFG power VS the product of mid-IR pumps powers at 80K

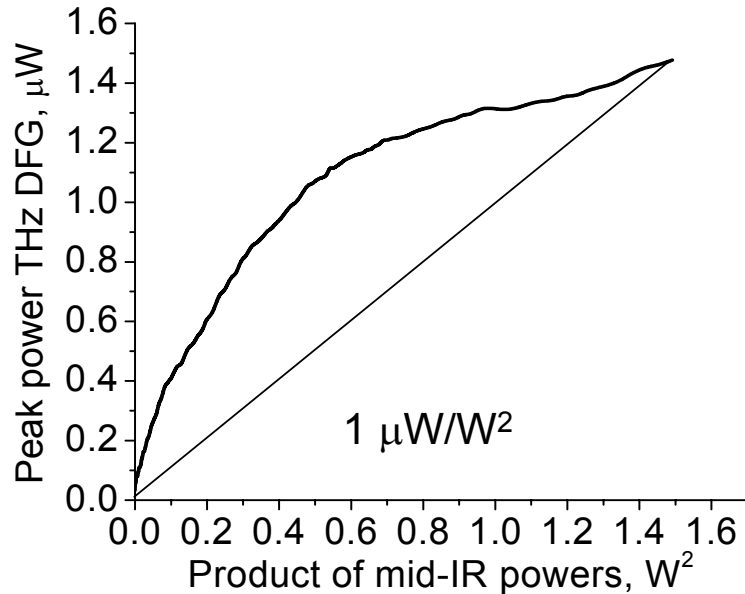


25-μm-wide, tapered to 50-μm-wide, 2-mm-long, back facet HR coating.
Testing in pulsed mode (60ns pulses at 250kHz).

THz power/conversion efficiency



THz DFG power VS the product of mid-IR pumps powers at 80K



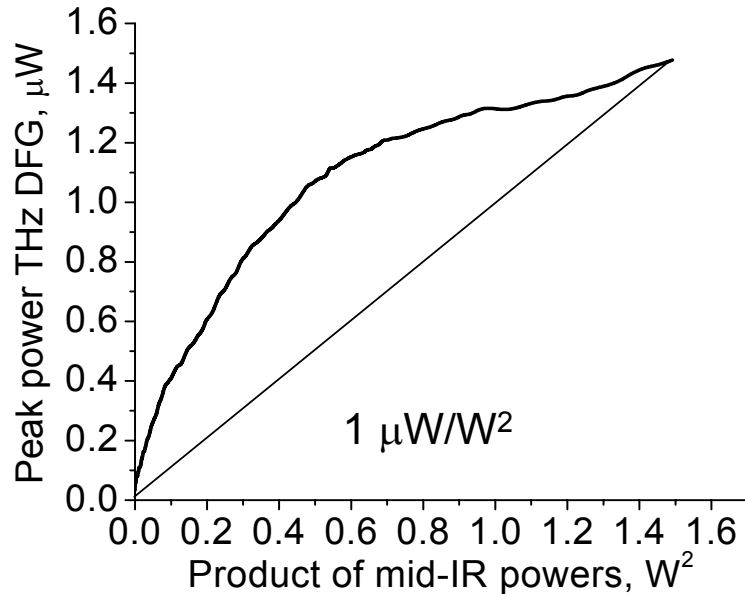
Conversion efficiency
~1 μW/W²

25-μm-wide, tapered to 50-μm-wide, 2-mm-long, back facet HR coating.
Testing in pulsed mode (60ns pulses at 250kHz).

THz power/conversion efficiency

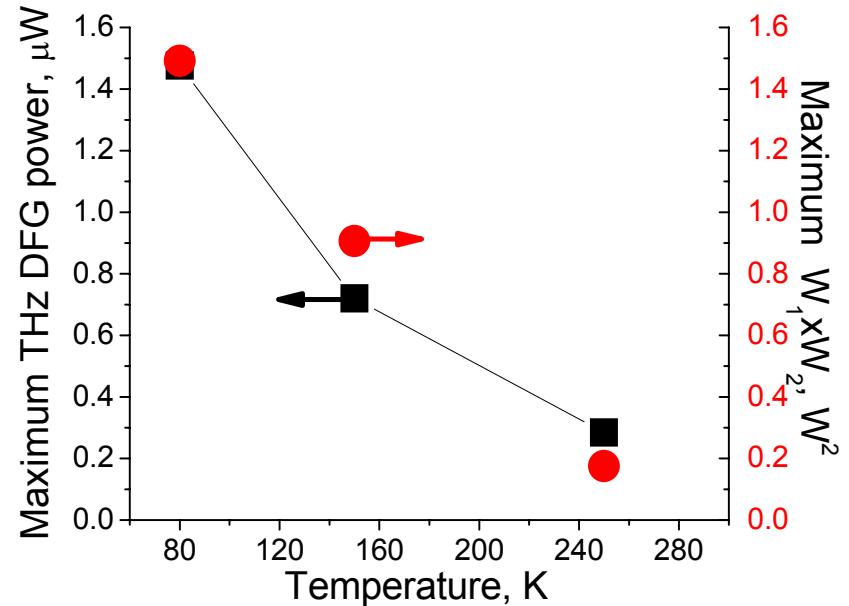


THz DFG power VS the product of mid-IR pumps powers at 80K



Conversion efficiency
 $\sim 1 \mu\text{W}/\text{W}^2$

Peak THz DFG power and mid-IR power versus temperature



THz DFG power scales with
pump powers at high
temperatures

25- μm -wide, tapered to 50- μm -wide, 2-mm-long, back facet HR coating.
Testing in pulsed mode (60ns pulses at 250kHz).

Conversion efficiency: analysis



$$W_{THz} \approx \frac{\omega^2}{8\epsilon_0 c^3 n_{eff}^\omega n_{eff}^{\omega_1} n_{eff}^{\omega_2}} \times \frac{|\chi^{(2)}|^2}{S_{eff}} W_1 W_2 \times l_{eff}^2$$

S_{eff} , l_{eff} , refractive indices are known from waveguide calculations:

$$n_{eff} \approx 3, l_{eff} \approx 90 \mu m, S_{eff} \approx 1800 \mu m^2$$

Estimate $\chi^{(2)}$ using electron density in upper laser state from gain=loss condition:

$$\chi^{(2)} \approx 4 \times 10^4 \text{ pm/V}$$

Uncertain parameters:

Mid-IR lasing in higher order lateral modes

THz wave out-coupling efficiency from QCL waveguide (~10%?)

Conversion efficiency: analysis



$$W_{THz} \approx \frac{\omega^2}{8\epsilon_0 c^3 n_{eff}^\omega n_{eff}^{\omega_1} n_{eff}^{\omega_2}} \times \frac{|\chi^{(2)}|^2}{S_{eff}} W_1 W_2 \times l_{eff}^2$$

S_{eff} , l_{eff} , refractive indices are known from waveguide calculations:

$$n_{eff} \approx 3, l_{eff} \approx 90 \mu m, S_{eff} \approx 1800 \mu m^2$$

Estimate $\chi^{(2)}$ using electron density in upper laser state from gain=loss condition:

$$\chi^{(2)} \approx 4 \times 10^4 \text{ pm/V}$$

Uncertain parameters:

Mid-IR lasing in higher order lateral modes

THz wave out-coupling efficiency from QCL waveguide (~10%?)

Theoretical efficiency: $W_{THz}/(W_1 \times W_2) \sim 10 \mu W/W^2$

Experiment (corrected for the collection efficiency): $\sim 1 \mu W/W^2$

**~10 times
discrepancy**

Future work



- *Attempt phase matching by varying waveguide width*
- *Improve edge emission out-coupling*
- *Surface emission scheme*
- *Novel active region designs*

Summary



- *Improved temperature performance and power of THz DFG in QCLs*
- *THz signal level is $>1\mu\text{W}$ at 80K and still $\sim 200\text{nW}$ at 250K*
- *Conversion efficiency is $\sim 1\mu\text{W}/\text{W}^2$.*
- *Large room for conversion efficiency improvements*

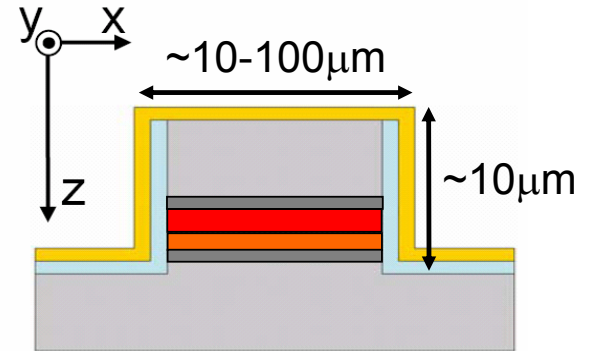
Funding: AFOSR

The structures were processed in the Center for Nanoscale Science (CNS) in Harvard University.

Surface emission scheme



- Only THz radiation generated within l_{eff} of the laser facet comes out of the device.
- Typical $l_{eff} \sim 100\mu\text{m}$; QCL length $\sim 3\text{mm}$
- Laser ridge height and width are smaller than THz wavelength \Rightarrow poor THz out-coupling



Surface emission

- Allows THz extraction along the whole device.
- Good THz beam quality.
- Out-coupling up to 30 cm^{-1}

